

# Radio-frequency-induced optical gain in $\text{Pr}^{3+}:\text{Y}_2\text{SiO}_5$

B. S. Ham and M. S. Shahriar

*Research Laboratory of Electronics, Massachusetts Institute of Technology, Cambridge, Massachusetts 02139*

P. R. Hemmer

*Air Force Research Laboratory, Hanscom Air Force Base, Massachusetts 01731*

Received October 6, 1997; revised manuscript received January 5, 1998

We report an observation of radio-frequency (RF) -induced transparency in an optically dense medium of  $\text{Pr}^{3+}$ -doped  $\text{Y}_2\text{SiO}_5$ . We observed that the optical probe field had a gain when the RF pulse area was  $2\pi$ . We also calculated the RF Rabi frequency in the medium by measuring the period of RF-induced transparency.

© 1998 Optical Society of America [S0740-3224(98)00705-X]

OCIS codes: 270.1670, 190.4720.

## 1. INTRODUCTION

In atom-field interactions, generally a weak laser pulse is absorbed gradually as it propagates through a resonant medium. However, an intense pulse shows very different absorption phenomena. In particular, if the pulse area  $A = 2n\pi$ ,  $n = 1, 2, 3, \dots$ , then the pulse propagates through the medium without any absorption in a two-level system. Therefore the medium appears to be transparent to the pulse, even though the light pulse is resonant with the atomic transition. Besides transparency, the pulse shape can be changed as the pulse propagates through the medium,<sup>1,2</sup> or the pulse can be broken up into several pulses.<sup>2-4</sup> This is called self-induced transparency.<sup>1-6</sup> Another type of transparency occurs in a three-level system where the interaction with two coherent fields can modify the absorption and the refractive index of the medium; thus the probe field is not absorbed at line center owing to destructive quantum interference. Therefore, an optically thick medium can become transparent. This is called electromagnetically induced transparency<sup>7-10</sup> (EIT). The difference between self-induced transparency and EIT is that in EIT the laser field is not absorbed by atoms owing to quantum interference. In self-induced transparency, however, emission cancels absorption; thus net absorption becomes zero. Recently, in solids, microwave and optical-field-induced transparencies were observed in ruby<sup>8</sup> (V-type) and in a rare-earth-doped crystal<sup>9,10</sup> ( $\Lambda$ -type), respectively.

In this paper we report radio-frequency-induced transparency (RFIT) in a ladder-type inhomogeneously broadened system of  $\text{Pr}^{3+}$ -doped  $\text{Y}_2\text{SiO}_5$  (Pr:YSO). The observed transparency is mostly due to the population change on the ground states caused by the radio-frequency (RF) field, and partly due to quantum interference in EIT. The detection of the RFIT was done by the method of optically detected nuclear magnetic resonance.<sup>11</sup> We also calculated the Rabi frequency of the RF pulse by measuring the period of the transparency

as a function of the RF pulse width. The direct measurement of the RF Rabi frequency is useful to optimize the experimental conditions for the EIT-related experiments. Finally we show a gain that is due to RFIT. We analyze this gain numerically and show that it is mostly due to population inversion of the optical transition. Assuming slow optical decay rate (or larger RF Rabi frequency than the optical decay rate), however, we show numerically that the optical gain is possible without population inversion with the RFIT. The observation of RFIT is important for applications such as frequency upconversion<sup>12,13</sup> or lasers without inversion<sup>14</sup> in solid media. In the area of frequency upconversion it has already been shown (in vapor) that vacuum-ultraviolet generation<sup>13</sup> is enhanced owing to EIT. In the area of lasers without inversion, low threshold semiconductor lasers with EIT have been proposed.<sup>15</sup>

Figure 1 shows the energy-level diagram of Pr:YSO. In our crystal the concentration of Pr ions is 0.05 at. %. One (site 1) of the two independent sites of YSO is chosen because of its large oscillator strength. The transition wavelength is  $\sim 606$  nm. The inhomogeneous width of the optical transition is  $\sim 4$  GHz at 1.6 K.<sup>16</sup> The optical population relaxation time  $T_1$  and transverse relaxation time  $T_2$  are 164  $\mu\text{s}$  and 111  $\mu\text{s}$ , respectively, at 1.6 K.<sup>16</sup> The ground-state spin  $T_1$  is of the order of 100 s,<sup>16</sup> and the spin  $T_2$  is 500  $\mu\text{s}$  at 6 K.<sup>17</sup> The laser field  $\omega_P$  in Fig. 1 is a probe for RFIT. The laser field  $\omega_R$  is a repump beam. In a persistent spectral hole-burning medium of Pr:YSO the repump modifies the probe absorption spectrum. In particular the repumped Pr ions have an effective optical line width limited by the inhomogeneous width of sublevel transitions and the laser jitter. Owing to the persistent spectral hole burning and the action of the repump, the six-level  $\text{Pr}^{3+}$  system can be simplified to a three-level system (energy levels  $|1\rangle$ ,  $|2\rangle$ , and  $|3\rangle$ ), shown in Fig. 1. In the absence of the RF field, most of the resonant Pr ions are accumulated on the state  $|1\rangle$  when both

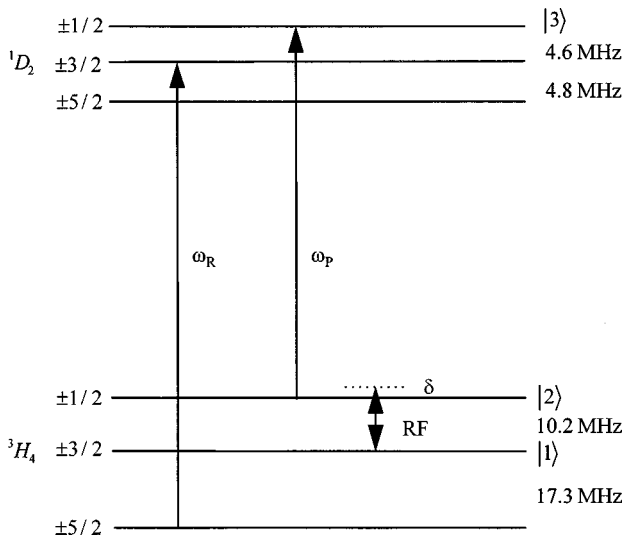


Fig. 1. Energy-level diagram of Pr:YSO.

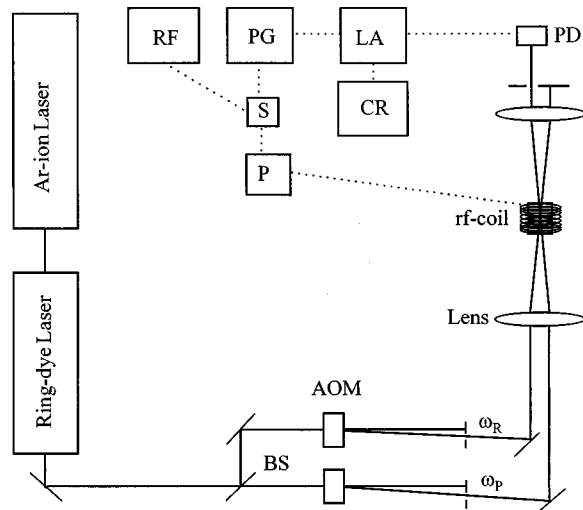


Fig. 2. Schematic of the experimental setup: AOM, acousto-optic modulator; BS, beam splitter; CR, chart recorder; LA, lock-in amplifier; P, RF power amplifier; PD, photodiode; PG, pulse generator; RF, RF frequency synthesizer; S, RF switch.

lasers  $\omega_P$  and  $\omega_R$  are on. Therefore the medium is transparent to the probe beam. If the RF field is resonant with the 10.2-MHz transition, it pumps the Pr ions from state |1> back into state |2>, and the probe beam is absorbed. This process is well known in optically detected nuclear magnetic resonance.<sup>11</sup>

## 2. EXPERIMENTAL SETUP

Figure 2 shows a schematic of the experimental setup. A frequency-stabilized cw ring dye laser is pumped by an argon-ion laser. For the frequency stabilization we lock the laser to a Fabry-Perot etalon having a 2-GHz free spectral range. We use acousto-optic modulators (AOM) driven by frequency synthesizers (PTS 160) to make two coherent laser beams from the dye-laser output, as shown. The laser beams are forward propagating and focused into the sample by a 40-cm focal-length lens. The angle between two laser beams is  $\sim 40$  mrad. The mea-

sured diameters of the beams are  $\sim 150 \mu\text{m}$  ( $1/e$  in intensity) in the crystal. The size of the crystal is 3 mm in diameter and 10 mm in length, and its crystal axes are unknown. For RF magnetic-field generation, a 24-turn copper coil is wound along the crystal length and mounted inside the cryostat. The temperature is kept at 6 K. The laser propagation direction is almost parallel to the RF coil axis, and the laser polarization is adjusted by a quarter-wave plate and a half-wave plate for maximum probe absorption. To generate RF pulses, we use a RF switch driven by a pulse generator (SRS DG 535). The RF pulse-repetition rate is 50 Hz, and the pulse width is variable. The probe signals are captured by a lock-in amplifier.

## 3. RESULTS

Figure 3 shows RF-induced Rabi flopping as a function of RF pulse width for different RF powers. As mentioned earlier, when the RF field is resonant with the 10.2-MHz transition, it pumps Pr ions from state |1> back into state |2>, increasing the probe absorption. Neglecting saturation, we expected that lower RF power should give weaker probe absorption. However, as the RF field remains turned on, the probe absorption dips as seen in Fig. 3. The transparency is explained by the area theorem in a

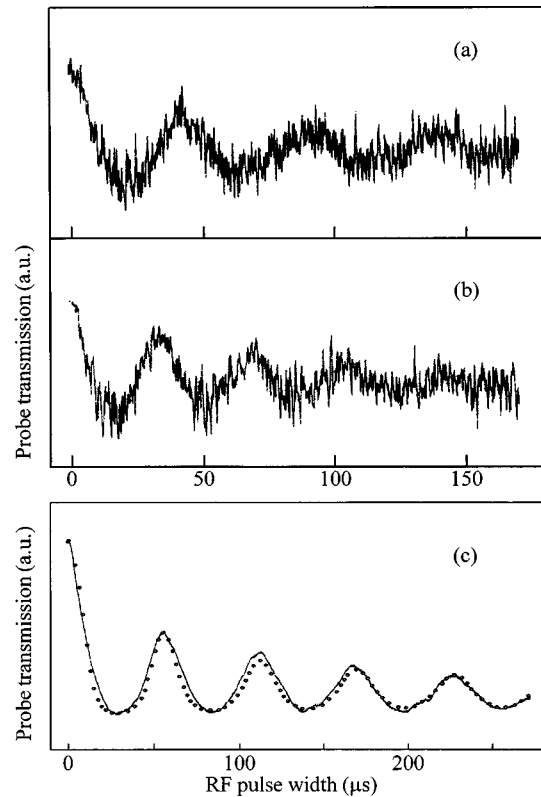


Fig. 3. (Experiment) Radio-frequency-induced transparency with RF powers of (a) 1.6 W, (b) 3.9 W, and (c) 1.2 W. The dotted curve in (c) is a numerical calculation;  $\Omega_P = 2$  kHz,  $\Gamma_P = 1$  kHz,  $\gamma_P = 100$  kHz,  $\Gamma_{RF} = 0$ ,  $\gamma_{RF} = 1$  kHz,  $\Delta_{inh} = 30$  kHz, and  $\Omega_{RF} = 17.6$  kHz, where  $\Omega$ ,  $\Gamma$ ,  $\gamma$  and  $\Delta_{inh}$  are Rabi frequency, population decay rate, phase decay rate, inhomogeneous width of the RF transition, and the subscripts P and RF stand for probe and RF transitions, respectively.

two-level system: The RF pulse inverts the population between the ground states when its area is  $\pi$ , giving a large optical absorption. When the pulse area is increased by another  $\pi$  (to  $2\pi$ ), it uninverts the population, giving transparency. As the RF pulse width increases more, the probe absorption oscillates with a particular period  $T$ . The oscillation periods are  $\sim 49 \mu\text{s}$  in Fig. 3(a) and  $\sim 36 \mu\text{s}$  in Fig. 3(b). From the measured oscillation period  $T$  we calculated the RF Rabi frequency  $\Omega$  by the area theorem,

$$\Omega T = 2\pi, \quad (1)$$

where  $\Omega \approx 21 \text{ kHz}$  in Fig. 3(a) and  $\Omega \approx 28 \text{ kHz}$  in Fig. 3(b). The oscillation period or the RF Rabi frequency can be varied by changing the applied RF power (or the number of the RF coil turns). Comparing Figs. 3(a) and 3(b) confirms that the oscillation period  $T$  is inversely proportional to the square root of the RF power. The absorption minima (or maxima) damp out as the RF pulse area increases. This is because each Pr ion has a slightly different Rabi frequency owing to inhomogeneous broadening on the  $|1\rangle$  to  $|2\rangle$  transition. The noise in the data is due to laser jitter.

To see the Rabi flopping at high optical density, we adjusted the wave plates for maximum probe absorption, gated the probe at the end of the RF pulse, and averaged it (30 samples) with a boxcar averager as a function of the RF pulse width [solid curve in Fig. 3(c)]. It should be noted that the boxcar averager is used for exact measurement of the optical density. With Eq. (1) the applied RF Rabi frequency is calculated to be 17.6 kHz from the oscillation period of the probe signal. For the calculation of optical density ( $\alpha l$ ), where  $\alpha$  is absorption coefficient and  $l$  is the length of the crystal, we solved density-matrix equations and plotted a best-fit curve to the probe absorption [dotted curve in Fig. 3(c)]. For the best-fit curve the optical density is 4. This can be compared with the expected optical density of 10 based on other work.<sup>16</sup> In the calculations we assumed an effective optical homogeneous width equal to the laser linewidth. The laser-jitter-induced line width is  $\sim 100 \text{ kHz}$  on time scales comparable to that of the  $10\text{-}\mu\text{s}$  RF pulse. To measure this, a Raman transition was excited between states  $|1\rangle$  and  $|2\rangle$  with time-delayed optical pulses, and the resulting spin coherence was monitored as a function of the delay time.

Figures 4(a)–4(d) show the probe-field absorption versus the RF detuning for different pulse widths of (a)  $35 \mu\text{s}$ , (b)  $40 \mu\text{s}$ , (c)  $45 \mu\text{s}$ , and (d)  $50 \mu\text{s}$  with the RF power used in Fig. 3(b). The laser powers are fixed at  $\sim 0.1 \text{ mW}$  for the probe and  $\sim 4 \text{ mW}$  for the repump. The FWHM of the absorption curves in Fig. 4 is  $\sim 100 \text{ kHz}$ , which is RF power broadened. We measured the inhomogeneous width of the 10.2-MHz RF transition to be  $\sim 30 \text{ kHz}$  using a weak cw RF field. Figure 4(a) shows RFIT, when the RF pulse area is  $2\pi$ . On line center of the absorption curve, the probe absorption is reduced because of the RFIT. The two symmetric absorption peaks are due to the reduction in effective pulse area with RF detuning. Generally, when the RF Rabi frequency is bigger than the line width of the  $|2\rangle - |3\rangle$  transition, the probe transparency should be large. However, the transparency on line center of Fig. 4(a) is degraded owing to laser jitter.<sup>18</sup> Fig-

ures 4(e)–4(h) are numerical calculations based on a three-level ladder-type system with parameters corresponding to Figs. 4(a)–4(d), respectively. The calculations approximately match the experimental data.

In Fig. 5(a) we show theoretical optical gains from RFIT. These plots were generated by solving the three-level density-matrix equations as a function of RF detuning for three different cases of optical homogeneous decay rates  $\gamma$ . We used parameters that were close to the experimental conditions. The RF pulse area was assumed to be  $2\pi$ , and the probe is assumed to be resonant. Figure 5(b) shows population difference ( $\rho_{33} - \rho_{22}$ ), which is the same for all three cases. Even though ground-state population is larger than the excited state at two-photon resonance (zero detuning of the RF), the probe can have gain from RFIT, if the decay rate  $\gamma$  is slow enough. Unfortunately, we have not experimentally seen this inversionless probe gain because of RF power limitation.

In Fig. 6 we observe a gain when the two laser intensities are increased by two orders of magnitude. Figure 6(a) shows the experimental probe absorption as a function of time, which is an average of ten waveforms. Figure 6(b) shows the numerical calculations; the solid curve is the probe absorption, and the dashed curve is the popu-

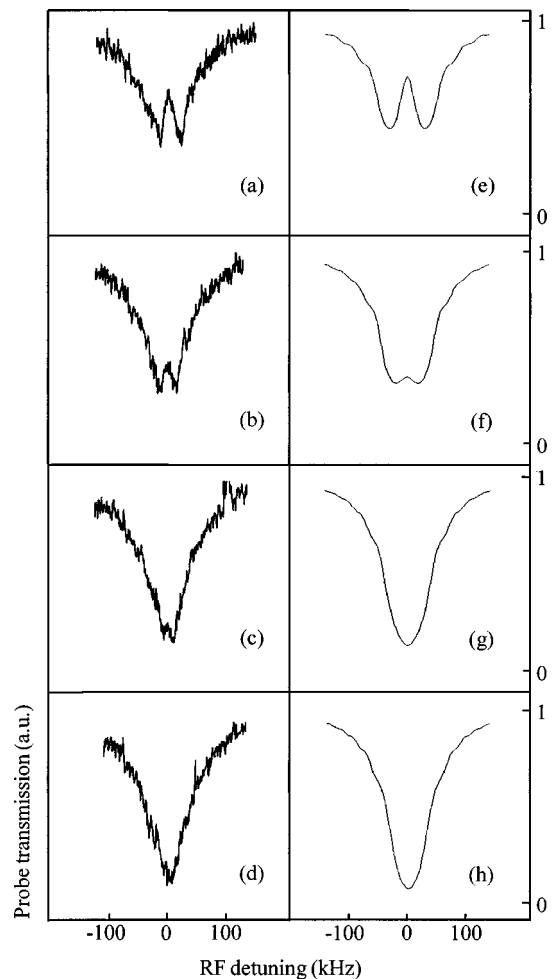


Fig. 4. Probe transmission versus RF detuning. RF pulse widths are (a)  $35 \mu\text{s}$ , (b)  $40 \mu\text{s}$ , (c)  $45 \mu\text{s}$ , and (d)  $50 \mu\text{s}$ . Numerical calculations of (e), (f), (g), and (h) are for (a), (b), (c), and (d), respectively.

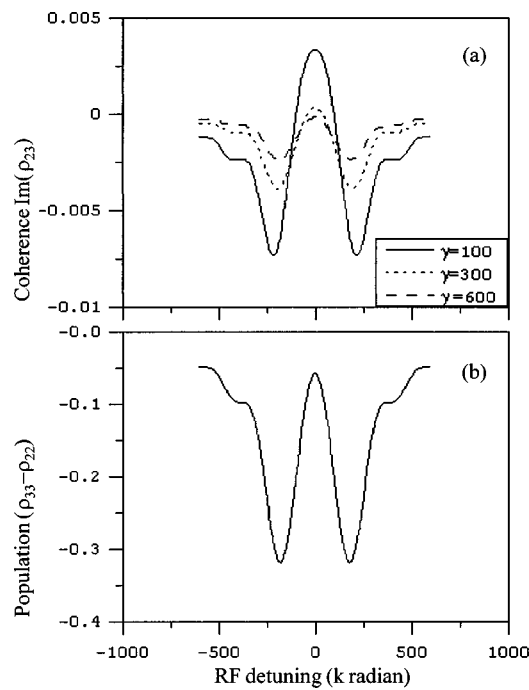


Fig. 5. Theoretically optical gain without population inversion: (a) Probe coherence  $\text{Im}(\rho_{23})$  and (b) population difference ( $\rho_{33} - \rho_{22}$ ) versus RF detuning;  $\Omega_P = 10$ ,  $\Omega_{RF} = 179$ ,  $\Gamma_P = 6$ ,  $\Gamma_{RF} = 0$ ,  $\gamma_{RF} = 4$ ,  $\Delta_{inh} = 100$  (kHz/2 $\pi$ ), and  $\gamma_P$  as shown.

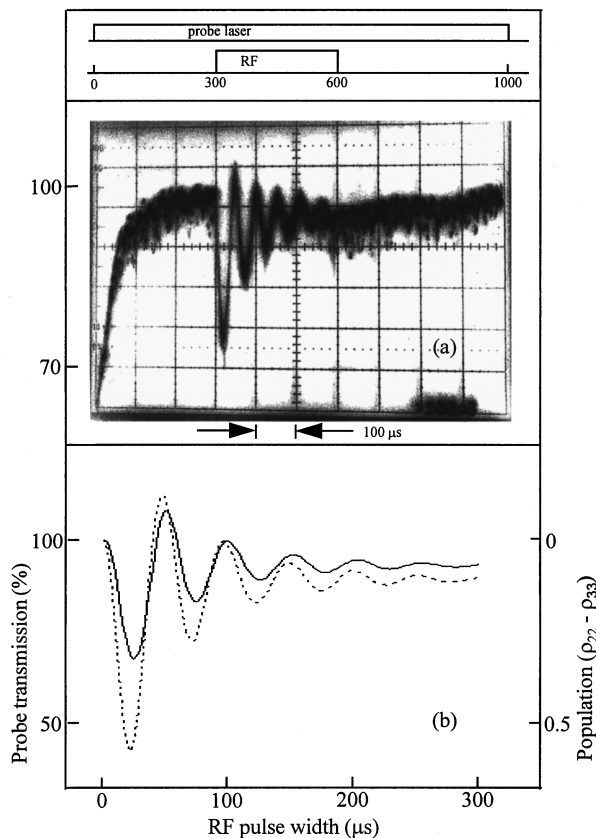


Fig. 6. Probe transmission versus time when the RF pulse is applied: (a) experiment and (b) theory;  $\gamma_P = 300$  kHz,  $\Omega_P = 16$  kHz,  $\Omega_{RF} = 28$  kHz, and  $\Delta_{inh} = 30$  kHz. Solid curve, probe transmission; dashed curve, population difference.

lation difference ( $\rho_{33} - \rho_{22}$ ). In Fig. 6(a) the RF pulse width is 300  $\mu\text{s}$ . At the end of the first  $2\pi$  RF Rabi oscillation there is an optical gain. This gain mostly comes from the population inversion ( $\rho_{33} > \rho_{22}$ ) [Fig. 6(b), dashed curve]. This occurs because the population initially in state  $|2\rangle$  is emptied by the RF  $2\pi$  pulse, but some population remains in  $|3\rangle$  after being deposited there by the probe laser before the RF pulse area reached  $2\pi$ . In the numerical calculations, if the laser jitter is reduced (or the RF power is increased), then gain is possible without population inversion, as seen in Fig. 5(a).

#### 4. CONCLUSION

In summary, we showed RFIT in a rare-earth-doped solid, Pr:YSO. The observed RFIT is mostly from the population change on the ground states and partially from quantum interference (EIT). We also showed a gain that is mostly due to population inversion on optical transition. In the experiment, the RF Rabi frequency was limited by the RF power amplifier to be less than the laser jitter; hence gain without population inversion was not observed. Nonetheless, these preliminary observations in a solid are important for EIT applications.

#### ACKNOWLEDGMENTS

We acknowledge discussions with S. Ezekiel of the Massachusetts Institute of Technology. This study was supported by Air Force Research Laboratory (grant F30602-96-2-0100) and the U.S. Air Force Office of Scientific Research (grant F49620-96-1-0395). The crystal was supplied by Scientific Material, Bozeman, Montana.

#### REFERENCES

1. S. L. McCall and E. L. Hahn, Phys. Rev. Lett. **18**, 908 (1967).
2. A. Szabo and N. Takeuchi, Opt. Commun. **15**, 250 (1975).
3. R. E. Slusher and H. M. Gibbs, Phys. Rev. A **5**, 1634 (1972).
4. L. McCall and E. L. Hahn, Phys. Rev. **183**, 457 (1969).
5. I. M. Asher and M. O. Scully, Opt. Commun. **3**, 395 (1971).
6. K. W. Smith and L. Allen, Opt. Commun. **8**, 166 (1973).
7. K.-J. Boller, A. Imamoglu, and S. E. Harris, Phys. Rev. Lett. **66**, 2593 (1991).
8. Y. Zhao, C. Wu, B. S. Ham, M. K. Kim, and E. Awad, Phys. Rev. Lett. **79**, 641 (1997).
9. B. S. Ham, M. S. Shahriar, and P. R. Hemmer, Opt. Lett. **22**, 1138 (1997).
10. B. S. Ham, P. R. Hemmer, and M. S. Shahriar, Opt. Commun. **144**, 227 (1997).
11. L. E. Erickson, Opt. Commun. **21**, 147 (1977).
12. K. Hakuta, L. Marmet, and B. P. Stoicheff, Phys. Rev. Lett. **66**, 596 (1991).
13. R. P. Blacewicz, M. G. Payne, W. R. Garrett, and J. C. Miller, Phys. Rev. A **34**, 5171 (1986).
14. O. A. Kocharovskaya and Y. I. Khanin, JETP Lett. **48**, 630 (1988); S. E. Harris, Phys. Rev. Lett. **62**, 1033 (1989); M. O. Scully and S. Y. Zhu, Phys. Rev. Lett. **62**, 2813 (1989).
15. Y. Zhao, D. Huang, and C. Wu, Opt. Lett. **19**, 816 (1994); A. Imamoglu and R. J. Ram, Opt. Lett. **19**, 1744 (1994).
16. R. W. Eqsall, R. L. Cone, and R. M. Macfarlane, Phys. Rev. B **52**, 3963 (1995).
17. B. S. Ham, M. S. Shahriar, M. K. Kim, and P. R. Hemmer, Opt. Lett. **22**, 1849 (1997).
18. Y.-Q. Li and M. Xiao, Phys. Rev. A **51**, 4959 (1995).